Published in final edited form as:
Invest Radiol. 2011 April ; 46(4): 215–224. doi:10.1097/RLI.0b013e3182034fed.

Ultrasound Molecular Imaging of Tumor Angiogenesis with an Integrin Targeted Microbubble Contrast Agent

Christopher R. Anderson, PhD[1,2,*], **Xiaowen Hu, BS**[2,*], **Jose Tlaxca, BS**[4], **Anne-Emilie Decleves, PhD**[5], **Robert Houghtaling**[4], **Kumar Sharma, MD**[5], **Michael Lawrence, PhD**[4], **Katherine Ferrara, PhD**[3], and **Joshua J. Rychak, PhD**[1]

[1] Targeson, Inc, San Diego, CA

[2] The College of New Jersey, Department of Biomedical Engineering, Ewing, NJ

[3] University of California, Davis, Department of Biomedical Engineering, Davis, CA

[4] University of Virginia, Department of Biomedical Engineering, Charlottesville, VA

[5] University of California San Diego, Division of Nephrology, San Diego, CA

Abstract

Rationale and Objectives—Ultrasound molecular imaging is an emerging technique for sensitive detection of intravascular targets. Molecular imaging of angiogenesis has strong potential for both clinical use and as a research tool in tumor biology and the development of anti-angiogenic therapies. Our objective is to develop a robust microbubble (MB) ultrasound contrast agent platform to which targeting ligands can be conjugated by biocompatible, covalent conjugation chemistry, and to develop a pure low mechanical index imaging processing method and corresponding quantifying method. The microbubbles and the imaging methods were evaluated in a mouse model of breast cancer *in vivo*.

Materials and Methods—We utilized a cyclic RGD (cRGD) pentapeptide containing a terminal cysteine group conjugated to the surface of MB bearing pyridyldithio-propionate (PDP) for targeting $\alpha_v\beta_3$ integrins. As negative controls, MB without a ligand or MB bearing a scrambled sequence (cRAD) were prepared. To enable characterization of peptides bound to MB surfaces, the cRGD peptide was labeled with FITC and detected by plate fluorometry, flow cytometry, and fluorescence microscopy. Targeted adhesion of cRGD-MB was demonstrated in an *in vitro* flow adhesion assay against recombinant murine $\alpha_v\beta_3$ integrin protein and $\alpha_v\beta_3$ integrin-expressing endothelial cells (bEnd.3). The specificity of cRGD-MB for $\alpha_v\beta_3$ integrin was demonstrated by treating bEnd.3 EC with a blocking antibody. A murine model of mammary carcinoma was used to assess targeted adhesion and ultrasound molecular imaging *in vivo*. The targeted microbubbles were visualized using a low mechanical index contrast imaging pulse sequence, and quantified by intensity normalization and two-dimensional Fourier transform analysis,

Results—The cRGD ligand concentration on the MB surface was ~8.2×10^6 molecules/MB. At a wall shear stress of 1.0 dynes/cm^2, cRGD-MB exhibited 5-fold higher adhesion to immobilized recombinant $\alpha_v\beta_3$ integrin relative to non-targeted MB and cRAD-MB controls. Similarly, cRGD-MB showed significantly greater adhesion to bEnd.3 EC compared to non-targeted MB and cRAD-MB. In addition, cRGD-MB, but not non-targeted MB or cRAD-MB, showed significantly enhanced contrast signals with a high tumor-to-background ratio. The adhesion of cRGD-MB to

Corresponding Author: Joshua Rychak, PhD, 3550 General Atomics Ct, MS 02 Room 444-445, San Diego, CA 92121, Joshua.rychak@targeson.com, Telephone: 877-290-4043 x 3, Fax: 973-273-5869.
*Both authors contributed equally to this manuscript

bEnd.3 was reduced by 80% after using anti-α_v monoclonal antibody to treat bEnd.3. The normalized image intensity amplitude was ~0.8 seven minutes after the administration of cRGD-MB relative to the intensity amplitude at the time of injection, while the spatial variance in image intensity improved the detection of bound agents. The accumulation of cRGD- MB was blocked by pre-administration with an anti-α_v blocking antibody.

Conclusion—The results demonstrate the functionality of a novel microbubble contrast agent covalently coupled to an RGD peptide for ultrasound molecular imaging of $\alpha_v\beta_3$ integrin and the feasibility of quantitative molecular ultrasound imaging with a low mechanical index.

INTRODUCTION

Angiogenesis, the growth of new blood vessels from existing vessels, is a fundamental component of tumor growth and metastasis[1]. Angiogenic endothelial cells exhibit drastic changes in the expression of cell surface molecules, including integrins that modulate cell adhesion, migration, and survival through interactions with the extracellular matrix[2]. A principle marker of the angiogenic phenotype is $\alpha_v\beta_3$ integrin, which is constitutively expressed in low levels in quiescent endothelial cells and highly upregulated during angiogenesis[3]. The $\alpha_v\beta_3$ integrin binds arginine-glycine-aspartic acid (RGD) sequences of provisional matrix proteins such as vitronectin and fibronectin. Blockade of $\alpha_v\beta_3$ integrin with monoclonal antibodies and small molecule antagonists has been shown to inhibit tumor angiogenesis in vivo[4,5]. Consequently, several therapeutic agents focused on the inhibition of $\alpha_v\beta_3$ integrin function are currently in clinical development[6,7].

Molecular imaging is a valuable tool that is being used increasingly in drug development, as it facilitates the characterization of target molecule expression levels in vivo and noninvasive evaluation of tumor responses to therapies[8–9]. The overexpression of $\alpha_v\beta_3$ integrin on the angiogenic endothelium provides a molecular target for delivery of imaging probes directly to the vasculature of growing tumors. Indeed, $\alpha_v\beta_3$ integrin has been targeted extensively for molecular imaging by several imaging modalities. Radiolabeled cyclic RGD peptides enabled evaluation of $\alpha_v\beta_3$ integrin expression in xenograft models of human melanoma[10] and various solid tumors in humans[11] with PET imaging. Paramagnetic nanoparticles and fluorescent quantum dots targeted to $\alpha_v\beta_3$ integrin have been used to image the tumor vasculature with MRI[12] and optical imaging[13], respectively. Additionally, contrast ultrasound imaging of human glioma xenografts expressing $\alpha_v\beta_3$ integrin has been demonstrated using microbubbles bearing the disintegrin echistatin[14].

Contrast ultrasound imaging is a compelling imaging technique, as it is inexpensive, portable, and permits real-time anatomical and molecular imaging[15]. Microbubble contrast agents are restricted to the vascular compartment due to their micron-scale diameter, which has important implications in the context of imaging tumor angiogenesis. Small molecule based imaging probes commonly used in other imaging modalities readily extravagate from the vasculature and are available to bind tumor cell markers as well. The $\alpha_v\beta_3$ integrin is highly expressed in many tumor cell types, and thus, ultrasound imaging of targeted microbubbles is unique in that it enables molecular imaging of $\alpha_v\beta_3$ integrin strictly on the angiogenic endothelium. The selectivity of $\alpha_v\beta_3$ integrin targeted microbubbles for the angiogenic endothelium could be useful in monitoring the effects of anti-angiogenic therapies on the tumor vasculature[16]. However, most previously described targeted microbubble designs use an avidin/biotin coupling scheme[16–22], which is not desirable for clinical use due to the potential for immunogenicity[23,24]. Here, we show that a cyclic RGD peptide can be covalently conjugated to a microbubble contrast agent by disulfide exchange chemistry, and demonstrate cRGD-MB adhesion to molecular and cellular substrates *in vitro*

and to the tumor vasculature *in vivo*. Further, we describe a novel image processing strategy for quantifying microbubble adhesion with contrast ultrasound imaging.

The most widely utilized method for contrast ultrasound molecular imaging[25–27] requires a combination of high and low-medium mechanical index (MI) pulses, where high MI pulses are used to destroy circulating microbubbles several minutes after injection. Quantification of adherent microbubbles is currently dependent on the injected microbubble dose, imaging system gain and local perfusion[28]. The development of quantitative, yet purely low MI, methods for ultrasound molecular imaging is desirable in order to facilitate the rapid translation of microbubble imaging to the clinic. In order to address these concerns, we propose an imaging method that employs low MI imaging pulses, normalization by the injected dose, averaging over a short (10 second) acquisition[29,30] and quantitative estimation of bound microbubbles. While many recent studies have optimized molecular imaging for pre-clinical ultrasound systems[21,22, 31,32] in conjunction with high MI pulses here, we optimize low MI signal processing for a sensitive clinical imaging system that does not require high MI pulses.

MATERIALS AND METHODS

Microbubble Preparation

An aqueous dispersion consisting of disteroylphosphatidylcholine (Avanti Polar Lipids; Alabaster, AL), distearoyl phosphatidylethanolamine-PEG 2000-pyridyl dithiopropionate (DSPE-PEG-PDP; Avanti), and PEG-40 stearate (Sigma, St. Louis, MO) was sonicated with an XL2020 probe sonicator (Misonix; Farmingdale, NY) while sparging with decafluorobutane (SynQuest; Alachua, Fl). A small amount (~2% by moles) of the fluorescent membrane probe DiI (Sigma Aldrich; St. Louis, MO) was included in the shell of some microbubble preparations for *ex vivo* detection by fluorescence microscopy. Unincorporated reactants were removed by several rounds of flotation. The concentration and size distribution of microbubble preparations were measured by electrozone sensing using a Coutler Multisizer II or IV (Beckman Coulter; Fullerton, CA) equipped with a 50 μm orifice. In some studies, a similar lipid microbubble without a conjugation residue was used (Targestar®-P; Targeson, San Diego, CA).

Ligand Conjugation

PDP bearing microbubbles were reacted with a cyclic RGD pentapeptide (cRGD; Peptides International, Louisville, KY). The cRGD ligand was thiolated and reacted with microbubbles at 5-fold molar excess relative to PDP groups for two hours at room temperature with gentle agitation. Control microbubbles bearing a scrambled sequence were prepared by reacting PDP-microbubbles with a thiolated cyclic RAD pentapeptide (cRAD). For some experiments, microbubbles were prepared with a FITC-labeled version of the cRGD peptide using the same conjugation method. Unbound ligand was removed by four rounds of centrifugal washing (400g for 4 min) in fluorocarbon-saturated saline. In some experiments, non-targeted microbubbles bearing PDP but no ligand were used as negative control.

Characterization of Labeled Microbubbles

FITC-labeled cRGD was used as a reporter for ligand conjugation to microbubble surfaces. The fluorescence of FITC-RGD labeled microbubbles was evaluated with a FACSCalibur flow cytometer (Becton-Dickinson, Franklin Lakes, NJ) as previously described[33], and also by fluorescence microscopy and spectroscopy. FITC labeled cRGD-MB were analyzed with electrozone sensing to determine the microbubble size and concentration. Microbubbles were then disrupted by sonication and heated at 65°C for ten minutes. The fluorescence of

the resulting dispersion, as well as serial dilutions of a FITC-cRGD standard, was assessed with a 96-well plate reader (Fluoroskan II). The fluorescence of the solution was then related to microbubble concentration to determine the ligand density on the microbubble surface.

Cell Culture

Murine brain endothelial cells (bEND.3; ATCC, Manassas, VA) were used to investigate microbubble adhesion to $\alpha_v\beta_3$ integrin expressing cell substrates. Cell-culture grade polystyrene dishes (Corning; Corning, NY) were precoated with 5 μg/cm^2 fibronectin for 2 hours at room temperature. Cells were grown to confluency in high-glucose Dulbecco's modified Eagle medium supplemented with 10% heat inactivated FBS and 1% penicillin-streptomycin (all from Gibco; Grand Island, NY). Cells were maintained at 37°C in a 95% air/ 5% CO_2 environment. The presence of $\alpha_v\beta_3$ integrin on endothelial surfaces was analyzed by flow cytometry after incubation with a PE-conjugated anti-murine α_v integrin monoclonal antibody (Clone RMV-7; Biolegend, San Diego, CA).

Parallel Plate Flow Chamber Adhesion Assay

PBS with 10 μg/ml recombinant human $\alpha_v\beta_3$ integrin (R&D Systems; Minneapolis, MN) was incubated on 35 mm non-treated polystyrene dishes overnight at 4°C. The following day, dishes were washed in PBS and non-specific adhesion was blocked by incubation with casein (Thermo Scientific; Waltham, MA) for 2 hours at room temperature. The dishes were inserted into an inverted parallel plate flow chamber (Glycotech; Rockville, MA). cRGD-MB were diluted to 5×10^6 MB/ml in saline with 0.2% BSA (Sigma-Aldrich; St. Louis, MO) and drawn through the flow chamber with a syringe pump (Harvard Apparatus; Holliston, MA) that was set to maintain a constant wall shear stress of 1.0 dyne/cm^2 over the substrates[57]. After 5 minutes, 15 fields of view were recorded using brightfield microscopy and a digital image acquisition system. As controls, cRGD-MB were drawn through the flow chamber in the presence of a recombinant $\alpha_v\beta_3$ integrin function blocking antibody at 20 μg/ml (Clone 23C6; R&D Systems), or cRGD-MB were drawn against casein-blocked surfaces. Additionally, these experiments were performed with microbubbles bearing the RAD control peptide.

Adhesion assays with bEND.3 endothelial cells were performed in a similar manner. Cells were grown to confluence in 35 mm polystyrene dishes, and cRGD MB or cRAD MB were diluted to 5×10^6 MB/ml in saline with 0.2% BSA and perfused over the cells in the flow chamber at 1.0 dyne/cm^2. In some experiments, cells were incubated with neutralizing antibodies at 20μg/ml for 30 minutes prior to adhesion assays in order to block α_v integrin (Clone RMV-7; Biolegend) or β_3 integrin (Clone 2C9.G2; Biolegend).

Mouse Model of Tumor Angiogenesis and Immunohistochemistry

All *in vivo* animal studies were approved by the Institutional Animal Care and Use Committee of the University of California, Davis. A total of 19 animals (female FVB mice, 6–7 weeks, 25–30 g, Charles River, MA) were examined during this study. Cells derived from the highly metastatic breast cancer Met-1[34] were transplanted into the 4th mammary fat pad and were allowed to grow for 10–14 days (mean diameter 5 mm) before ultrasound imaging or tissue harvest. For histochemical analysis, tumor samples were fixed in formalin solution, embedded in paraffin, and then sliced into 5-μm sections using a microtome. Samples were stained using Hematoxylin & Eosin and an anti-murine CD51 monoclonal antibody (Clone RMV-7; BioLegend, San Diego, CA) to visualize tumor morphology and vasculature structure, respectively. Fluorescence immunostaining was performed on frozen tumor sections. An overlay was carried out with the primary antibodies (rabbit anti-Integrin beta3; Millipore and rat anti-CD31 antibody; Serotec). Images were captured by confocal laser fluorescence microscope at X63 original magnification (Zeiss LSM 510).

Microbubble Imaging and Inhibition Studies

The skin above and around the tumor was shaved and further treated with depilatory (Veet, Reckitt Benckiser) in order to fully remove all fur. Ultrasound gel (Aquasonic, Parker Laboratories Fairfield, NJ) was used to couple the ultrasound transducer. Mice were anesthetized with 2% isoflurane (Halocarbon Laboratory, River Edge, NJ) in oxygen (2 L/min) and placed on a heated stage to maintain body temperature at 37°C. Microbubbles were administered by tail vein injection with a 27 gauge needle connected to a cannula, and the maximum injection volumes were limited to 250 μL per mouse. A dose of 1×10^8 microbubbles were injected into the tail vein and followed with a 10 μL saline flush. Acute toxicity was not observed in any animals.

Boluses of cRGD-MB and either cRAD-MB (n=6) or non-targeted MB controls (n=4) were injected and imaged in random order. A 5-minute delay was added between imaging sessions and a destructive pulse was implemented to eliminate microbubbles from the preceding study. In some mice, a monoclonal antibody against murine CD51 (Clone RMV-7; BioLegend, San Diego, CA) was administered in order to block $\alpha_v\beta_3$ integrin. These mice (n=6) were first administered cRGD-MB as above in order to assess baseline MB adhesion, followed by injection of 100μg of anti-CD51 antibody through the tail vein cannula five minutes later. Thirty minutes after antibody administration, cRGD-MB were administered again and mice were imaged again to assess cRGD-MB adhesion. In other inhibition experiments, soluble cRGD peptide (400 μg; n=10) was used in order to block cRGD-MB adhesion.

Contrast Ultrasound Imaging

Ultrasound imaging was performed with a Sequoia 512 (Siemens, Issaquah, WA) system using a 15L8-S high frequency linear transducer operating in contrast pulse sequencing (CPS) mode at 7 MHz. In brief, CPS imaging transmits three pulses with varied amplitude and phase, and then produces the summation of the corresponding echoes[35]. CPS imaging settings were optimized as follows in order to minimize tissue clutter and broadband noise. The transmitted power for CPS pulses was −27 dB, which corresponded to an MI of 0.09 and an approximate peak negative pressure of ~230kPa. The frame rate was 11 Hz, CPS gain was 5 and the dynamic range was 65 dB. The acoustic focal zone was placed at the center of the tumor at the largest transverse cross section. A field of view encompassing the tumor and adjacent tissue deep and lateral to the tumor was acquired.

The imaging protocol used in this study was designed to distinguish the contrast echoes from target-bound microbubbles from those arising from freely-circulating microbubbles. Thirty seconds after microbubble administration, a 10-second CPS imaging sequence was acquired in order to observe the contrast echoes from both bound and free microbubbles during the wash-in of the agents through the tumor and adjacent tissue. Ultrasound transmission was then paused for 7 minutes to allow time for accumulation of microbubbles at the target site and clearance of unbound microbubbles. After 7 minutes, a second 10-second CPS imaging sequence was acquired. To confirm that the signal acquired at 7 minutes was primarily from target-bound microbubbles, a high MI (MI=1.9, center frequency ~5MHz) destructive pulse of duration 2 seconds was delivered in order to destroy all microbubbles within the ultrasound field. Thirty seconds after the destructive pulse, a final 10-second CPS imaging sequence was acquired in order to observe any replenishment of circulating microbubbles.

Ex vivo confocal fluorescent imaging of microbubble accumulation

DiI-labeled cRGD microbubbles were injected into the tail vein of mice with bilateral MET-1 tumors that were roughly 5 mm in diameter. Tumors were imaged after 7 minutes as

described above. After an additional 5 minutes, fluorescein-labeled *Lycopersicon esculentum* (Tomato) Lectin (VectorLab, Burlingame, CA) was injected intravenously (50 μg/mouse) in order to delineate the vascular endothelium. Animals were sacrificed five minutes after lectin administration, and tumors were harvested and snap frozen. Control tumors were harvested from animals that were treated with lectin, but did not receive injection of DiI-cRGD microbubbles. All tumors were imaged with the Marianas System (Intelligent Imaging Innovations Inc., Denver, CO), using Slidebook (Intelligent Imaging Innovations Inc., Denver, CO) on an AxiObserver microscope (Carl Zeiss, Oberkochen, Germany). Images were acquired with a CoolSNAP HQ2 camera (Roper Scientific Inc., Tucson, AZ) and spinning disk confocal CSU10 system (Yokogawa, Tokyo, Japan) at 40X (NA 1.1). Lectin and DiI were excited at 488/561 nm, respectively.. For each tumor, 5 z-stacks of images (200 μm×200 μm× (10–20) μm each z-stack) were recorded, and blood vessels stained by lectin were identified. All images were analyzed with Slidebook or ImageJ.

Image Analysis

All ultrasound image sequences were recorded digitally and analyzed offline with MATLAB® (Mathworks, Natick, MA). Sum-absolute-difference (SAD) motion tracking was performed prior to the image analysis and 50 aligned CPS images were averaged on a pixel-by-pixel basis. Quantitative image intensity measurements were then made over manually-selected region of interests (ROI) on the averaged images. The average image intensity over an ROI encompassing the tumor was calculated for each 10-second image acquisition sequence. The image intensity measured at the 7-minute time point was normalized by the peak intensity immediately following MB injection for each animal. This ratio was used to scale each pixel of the image at the 7-minute time point, in order to account for potential variation in injected contrast volume or vascular delivery of microbubbles to the tumor. Digital subtraction of the post-destruction sequence was also applied to pre-destruction sequences to evaluate the contribution of high-MI destruction pulses to the differentiation of free and bound microbubbles. Additionally, the two-dimensional Fourier transform of the 10-second averaged and normalized images was performed in MATLAB®. The breadth of spatial frequencies present in the images was estimated by the two-sided -6 dB spectral width. The Fourier based method for estimating microbubble accumulation was verified in vitro. Figure 4 illustrates the imaging strategy used here to investigate the adhesion of cRGD-MB to the angiogenic endothelium in the Met-1 tumor model.

Statistical Analysis

Wilcoxon rank sum test were performed to compare normalized contrast intensity, with each mouse serving as its own control in repeated injections of targeted and control agents. A *p*-value below 0.05 was considered significant. The number of mice required for each set of experiments was determined by power analysis. In the first experimental set, a sample size of 4 mice was calculated in order to detect an estimated 20% difference between cRGD and untargeted control microbubbles (10% standard deviation, $\alpha = 0.05$, power of 0.8). In the second experimental set, a sample size of six was chosen to detect a smaller predicted change between cRGD-MB and cRAD-MB, and in response to the administration of blocking antibodies. The evaluation of specificity following the administration of soluble peptides was tested with n=10 animals.

RESULTS

Characterization of cRGD Microbubble Contrast Agents

All of the microbubbles used in this study had a mean diameter of approximately 2.5 μm, with less than 2% of diameter above 8 um. Table 1 shows summary parameters of cRGD and control cRAD microbubbles measured by electrozone sensing, and a representative size distribution is shown in Figure 1B. We used FITC-labeled cRGD peptides as a reporter for characterizing the extent of ligand conjugation to PDP-bearing microbubbles. The conjugation of FITC-cRGD to microbubble surfaces was analyzed with fluorescence spectroscopy, flow cytometry, and fluorescence microscopy (Figure 1). Conjugation of FITC-cRGD to PDP-MB saturated at a 5-fold molar excess of FITC-RGD relative to PDP reactive groups, resulting in 8.2 +/− 1.6 × 10^6 cRGD peptides per microbubble (Figure 1A), as assessed by fluorescence spectroscopy. In contrast, control microbubbles without PDP reactive groups bound <1000 FITC-cRGD peptides per microbubble. The presence of FITC-cRGD bound to PDP-bearing microbubbles was confirmed by flow cytometry (Figure 1C) and fluorescence microscopy (Figure 1D).

Recombinant $\alpha_v\beta_3$ integrin and endothelial cell substrates were used to investigate the adhesion of cRGD-MB (Figure 2). cRGD-MB or control cRAD-MB were infused through a parallel plate flow chamber coated with a substrate of recombinant human $\alpha_v\beta_3$ integrin, or, as a negative control, a casein blocking solution. Significantly greater adhesion to $\alpha_v\beta_3$ integrin target surfaces compared to casein control surfaces was observed for cRGD-MB (Figure 2A). To demonstrate that cRGD-MB adhesion was due to molecular interactions with $\alpha_v\beta_3$ integrin, the target surface was incubated with a neutralizing antibody to block $\alpha_v\beta_3$ integrin function. The adhesion of cRGD-MB to recombinant $\alpha_v\beta_3$ integrin substrates (37.5 +/− 9.2 MB/FOV) was significantly higher than casein surfaces (0.7 +/− 0.5 MB/FOV) and antibody blocked $\alpha_v\beta_3$ integrin surfaces (3.9 +/− 1.5 MB/FOV) (Figure 2B). cRAD-MB control exhibited minimal adhesion to both $\alpha_v\beta_3$ integrin and casein surfaces. Control microbubbles bearing PDP alone without any ligand did not exhibit any adhesion to target substrates (data not shown).

Murine brain endothelial cells (bEnd.3) expressing $\alpha_v\beta_3$ integrin were used to investigate cRGD-MB adhesion to a cellular substrate under the same flow conditions. The presence of $\alpha_v\beta_3$ integrin on the surface of bEnd.3 cells was confirmed by flow cytometry (Figure 2C). cRGD-MB exhibited over a five-fold increase in adhesion to endothelial cells relative to cRAD-MB or non-targeted control MB (Figure 2D). Adhesion of cRGD-MB was abrogated by the incubation of endothelial cells with antibodies that block the function of either the α_v or β_3 integrin subunits.

Ultrasound Imaging of Tumor Angiogenesis In Vivo

Contrast ultrasound imaging was performed on mice bearing Met-1 mammary carcinoma tumors two weeks after inoculation. Representative ultrasound images of a typical tumor are shown in Fig 3A (B-mode, showing tumor size and borders) and 3B (baseline CPS image, shown lack of contrast signal before agent administration). The Met-1 tumor is a syngeneic tumor model growing within the mammary fat pad (Figure 3C) and elicits significant angiogenesis, as demonstrated by the high vascular density marked by α_v-integrin (CD51) expressing blood vessels (Figure 3D). Representative confocal microscopy images of the vasculature in tumors from DiI-cRGD-microbubble-treated animals demonstrate the accumulation of targeted within the vasculature (Fig. 3E-F). No microbubbles were observed outside the vasculature demarcated by FITC-lectin staining, suggesting that microbubbles are binding a target on the luminal endothelium of the tumor.

Representative ultrasound images of cRGD-MB within a tumor are shown in Figure 5. The unprocessed CPS image acquired immediately after microbubble administration shows enhancement throughout the tumor and within the adjacent tissue (Figure 5A). Contrast enhancement within the tumors is visible after 7 minutes (Figure 5B), with minimal signal in the (presumably non-angiogenic) adjacent tissue (yellow circles). The microbubble echo amplitude acquired 30 seconds after transmission of a high-power destruction sequence (Fig 5C) was minimal, indicating the absence of circulating microbubbles within the ultrasound field 7 minutes after injection. Additionally, the lack of signal after microbubble destruction illustrates the high contrast-to-tissue ratio achieved with CPS imaging of cRGD-MB in this model.

Averaging over the 10-second acquisition period further decreases the image amplitude within the peri-tumoral vasculature at the 7-minute time point (circled in Figure 5B, E)[36]. The 10-second integration performed at the time of injection results in a smoothed image of the tumor due to the presence of moving microbubbles perfusing the tumor (Figure 5D, G); however, the application of frame integration and normalization at the 7 minute time point results in a speckled image, due to the presence of primarily adherent microbubbles (Figure 5H). The speckled spatial variance of the averaged images is estimated by calculating the two-dimensional Fourier transform of the time-averaged images (Figure 5J, K). The center of the 2D FT image is the origin of frequency domain, with lower frequency components closer to the center and higher frequency components near the boundaries. The breadth of spatial frequency content within images acquired 7 minutes after injection was 2.72±0.15 cycles/mm, which was significantly greater than that calculated immediately after injection (0.76±0.11 cycles/mm).

In vitro phantom experiments verified the difference in two-dimensional Fourier transform images between freely circulating microbubbles and bound microbubbles (data not shown), and the *in vitro* spatial frequencies associated with bound and free microbubbles were 2.8 and 0.8 cycles/mm, respectively. This measurement is gain-insensitive, as we verified that the breadth of spatial frequencies changed by less than 5% as the gain changed from −20dB to −10dB.

The average intensity of the CPS signal within the tumor acquired 7 minutes after the administration of cRGD-MB was ~80% of the intensity calculated at the time of injection (Figure 6), which suggests that not all of the administered contrast is retained within the tumor. This is to be expected, as MB are retained only within regions of the tumor that express the specific molecule targeted here. After 7 minutes, the average image intensity of tumors after cRGD-MB administration was 33- and 7-fold greater than the image intensity observed with non-targeted MB and cRAD-MB, respectively (Figure 6A). Conversely, cRGD-MB did not lead to a substantial image intensity in surrounding vessels or tissue. Pixel-by pixel subtraction of the post-destruction image from the pre-destruction image at 7 minutes amplitude did not significantly change the magnitude of the average image intensity (Figure 6B), which suggests that the dwell time of 7 minutes was sufficient for clearance of the majority of circulating microbubbles. The specificity of cRGD-MB for $\alpha_v\beta_3$ integrin on the tumor endothelium was demonstrated by pre- treatment with an α_v -neutralizing antibody. The image intensity resulting from cRGD-MB was reduced by 3.2 fold after the administration of the blocking antibody (Figure 6F). However, pre-treatment with soluble cRGD peptides did not attenuate the image intensity of cRGD-MB within the tumor vasculature (Figure 6G).

DISCUSSION

Targeted contrast ultrasound imaging provides a convenient and noninvasive technique for characterizing and evaluating biological processes in vivo. In the context of tumor growth, ultrasound molecular imaging enables the detection of angiogenesis[14,21–22,37–40] and the monitoring of responses to anti-angiogenic therapies[16]. To this end, microbubble contrast agents have been conjugated to ligands specific for highly expressed molecular markers of tumor angiogenesis such as VEGFR-2[21–22,39–40, 54] and $\alpha_v\beta_3$ integrin[14,41–43]. Microbubbles targeted to $\alpha_v\beta_3$ integrin have resulted in significant ultrasound signal enhancements in several tumor models[14,41]; however, previously described agents utilize biotin/streptavidin interactions to conjugate targeting ligands, which introduces several drawbacks. Streptavidin has been shown to mediate non-specific adhesion to endothelial cellsvia interactions with endogenous fibronectin[44]. Furthermore, the administration of streptavidin[23] or streptavidin-antibody conjugates[24] resulted in elevated plasma levels of human anti-streptavidin antibodies in the clinical investigation of radioimmunotherapies for tumor treatment. Thus, covalent conjugation of a cyclic RGD peptide circumvents the potential non-specific adhesion and immunogenicity of streptavidin-based microbubbles and provides a significant advance in targeted microbubble design.

Functional adhesion of cRGD-MB to the angiogenic endothelium in vivo was demonstrated with a mouse model of mammary carcinoma. The accumulation of adherent cRGD-MB within the tumor vasculature was observed by contrast ultrasound imaging seven minutes after administration, which was sufficient to clear unbound microbubbles from the circulation. The MI of the imaging pulses in this study was 0.09, which minimized the fragmentation of adherent agents. Averaging over 50 frames retained echoes from adherent agents and suppressed echoes from free agents, improving the quantitation of bound agents.

To quantify the extent of cRGD-MB adhesion, we normalized the image intensity amplitude after seven minutes by the amplitude at the time of injection. This normalization approach accounts for changes in the number or size of contrast agents reaching the tumor, and will be particularly helpful if the ROI has low expression of the target receptor. After seven minutes, the normalized image intensity value for tumors injected with cRGD-MB was ~0.8, which was significantly greater than the values observed for tumors injected with non-targeted and cRAD-MB control agents. Importantly, the cRGD-MB normalized image intensities were unchanged after pixel-by-pixel subtraction of the post-microbubble destruction image intensities. This suggests that this imaging approach is particularly suitable for clinical translation as quantifying adhesion without microbubble destruction is desirable.

In[45–47] high-MI imaging was shown to improve the detection sensitivity of bound microbubbles. High sensitivity imaging is particularly desirable for small diameter microbubbles or a low receptor and therefore microbubble density. However, high MI pulse sequences have been associated with premature ventricular contractions, sonoporation and cell membrane damage, particularly when microbubbles are in contact with the membrane[48–53]. Although such effects are not expected to result in significant or long-lasting biological effects, use of a low MI pulse sequence can avoid the potential for such complications in future human studies.

Specificity of cRGD-MB for $\alpha_v\beta_3$ integrin on the endothelium was demonstrated by the significant attenuation in image intensity after pre-administration of an α_v-integrin blocking antibody. Both the *in vitro* adhesion assay on cells and the *in vivo* experiments suggest that approximately 75% of the cRGD-MB adhesion is due to adhesion through the $\alpha_v\beta_3$ integrin. We have not identified the mechanism behind the residual adhesion. However, RGD-based

constructs are known to bind to various integrins[4,5], and we hypothesize that one or more integrins expressed on tumor endothelium is responsible. In addition, the RGD motif is also known to have affinity for the GPIIB/IIIa expressed on activated platelets, which is another potential target for microbubble adhesion, albeit unwanted in the context of targeting angiogenesis. In the current study we have not specifically excluded cRGD-MB adhesion to platelets. We do note, however, that platelet aggregation does not appear to have been observed in previous studies using RGD-based imaging constructs.

We observed that pre-administration of soluble cRGD peptide, unlike blocking antibody, did not abrogate MB adhesion within the tumor. This could be due to several mechanisms. First, the cRGD-MB described here present multiple copies of the cRGD ligand simultaneously. This configuration encourages cooperative multi-point interaction, leading to a greater adhesion force than that encountered for single soluble molecules.[55] Additionally, clustering or multi-valency has been shown to be important for high-efficiency binding cRGD targeting peptides[56]. These mechanisms may explain why free peptide, with expected affinity in the micromolar range, did not block adhesion of the cRGD-MB *in vivo*. Finally, the low molecular weight cRGD peptide may readily extravasate from the intravascular space such that the local concentration of the cRGD peptide is insufficient for blocking $\alpha_v\beta_3$ integrin on the endothelial surface.

The results of this study demonstrate that cRGD-MB bind $\alpha_v\beta_3$ integrin with good specificity and facilitate the quantitative visualization of tumor angiogenesis by contrast ultrasound imaging. These results also support the use of low MI ultrasound scanning strategies and corresponding image processing schemes for quantifying the magnitude of cRGD-MB accumulation in tumor tissues. This technique may be of significant utility in the field of molecular imaging, both in the setting of research and clinical practice.

Acknowledgments

The authors are grateful for assistance from Geoffrey Parks, Dan Smith, Emily Smith and Lisa Mahakian and acknowledge equipment support from Siemens Medical Solutions. The authors would also like to thank Dr. Soichiro Yamada for his assistance with confocal microscopy. This study was supported by NIH 1R43CA137913 to C.R.A., NIH CA134659, CA112356, and CA103828 to KWF, and NIH EB007857 to J.J.R.

Source of Support: NIH 1R43CA137913 to C.R.A., NIH 2R44EB007857 to J.J.R., NIH CA 134659 to KWF, NIH CA 112356 to KWF, NIH CA 103828 to KWF

References

1. Carmeliet P, Jain RK. Angiogenesis in cancer and other diseases. Nature. 2000; 407:249–57. [PubMed: 11001068]
2. Stupack DG, Cheresh DA. Apoptotic cues from the extracellular matrix: regulators of angiogenesis. Oncogene. 2003; 22:9022–9. [PubMed: 14663480]
3. Brooks PC, Clark RA, Cheresh DA. Requirement of vascular integrin alpha v beta 3 for angiogenesis. Science. 1994; 264:569–571. [PubMed: 7512751]
4. Brooks PC, Montgomery AM, Rosenfeld M, et al. Integrin alpha v beta 3 antagonists promote tumor regression by inducing apoptosis of angiogenic blood vessels. Cell. 1994; 79:1157–64. [PubMed: 7528107]
5. Brooks PC, Stromblad S, Klemke R, et al. Antiintegrin alpha_v beta_3 blocks human breast cancer growth and angiogenesis in human skin. J Clin Invest. 1995; 96:1815–22. [PubMed: 7560073]
6. Nabors LB, Mikkelsen T, Rosenfeld SS, et al. Phase I and correlative biology study of cilengitide in patients with recurrent malignant glioma. J Clin Oncol. 2007; 25:1651–7. [PubMed: 17470857]
7. McNeel DG, Eickhoff J, Lee FT, et al. Phase I trial of a monoclonal antibody specific for alphavbeta3 integrin (MEDI-522) in patients with advanced malignancies, including an assessment of effect on tumor perfusion. Clin Cancer Res. 2005; 11:7851–60. [PubMed: 16278408]

8. Weber WA, Czernin J, Phelps ME, et al. Technology Insight: novel imaging of molecular targets is an emerging area crucial to the development of targeted drugs. Nat Clin Pract Oncol. 2008; 5:44–54. [PubMed: 18097456]
9. Cai W, Rao J, Gambhir SS, et al. How molecular imaging is speeding up antiangiogenic drug development. Mol Cancer Ther. 2006; 5:2624–33. [PubMed: 17121909]
10. Haubner R, Wester HJ, Weber WA, et al. Noninvasive imaging of alpha(v)beta3 integrin expression using 18F-labeled RGD-containing glycopeptide and positron emission tomography. Cancer Res. 2001; 61:1781–5. [PubMed: 11280722]
11. Beer AJ, Haubner R, Sarbia M, et al. Positron emission tomography using [18F] Galacto-RGD identifies the level of integrin alpha(v)beta3 expression in man. Clin Cancer Res. 2006; 12:3942–9. [PubMed: 16818691]
12. Winter PM, Caruthers SD, Kassner A, et al. Molecular imaging of angiogenesis in nascent Vx-2 rabbit tumors using a novel alpha(nu)beta3-targeted nanoparticle and 1.5 tesla magnetic resonance imaging. Cancer Res. 2003; 63:5838–43. [PubMed: 14522907]
13. Cai W, Shin DW, Chen K, et al. Peptide-labeled near-infrared quantum dots for imaging tumor vasculature in living subjects. Nano Lett. 2006; 6:669–76. [PubMed: 16608262]
14. Ellegala DB, Leong-Poi H, Carpenter JE, et al. Imaging tumor angiogenesis with contrast ultrasound and microbubbles targeted to alpha(v)beta3. Circulation. 2003; 108:336–341. [PubMed: 12835208]
15. Klibanov AL. Ligand-carrying gas-filled microbubbles: ultrasound contrast agents for targeted molecular imaging. Bioconjug Chem. 2005; 16:9–17. [PubMed: 15656569]
16. Korpanty G, Carbon JG, Grayburn PA, et al. Monitoring response to anticancer therapy by targeting microbubbles to tumor vasculature. Clin Cancer Res. 2007; 13:323–30. [PubMed: 17200371]
17. Lindner JR, Song J, Christiansen J, et al. Ultrasound assessment of inflammation and renal tissue injury with microbubbles targeted to P-selectin. Circulation. 2001; 104:2107–12. [PubMed: 11673354]
18. Linker RA, Reinhardt M, Bendszus M, et al. In vivo molecular imaging of adhesion molecules in experimental autoimmune encephalomyelitis (EAE). J Autoimmunity. 2005; 25:199–205. [PubMed: 16249069]
19. Weller GE, Lu E, Csikari MM, et al. Ultrasound imaging of acute cardiac transplant rejection with microbubbles targeted to intercellular adhesion molecule-1. Circulation. 2003; 108:218–224. [PubMed: 12835214]
20. Korpanty G, Grayburn PA, Shohet RV, et al. Targeting vascular endothelium with avidin microbubbles. Ultrasound Med Biol. 2005; 31:1279–83. [PubMed: 16176794]
21. Willmann JK, Paulmurugan R, Chen K, et al. US imaging of tumor angiogenesis with microbubbles targeted to vascular endothelial growth factor receptor type 2 in mice. Radiology. 2008; 246:508–18. [PubMed: 18180339]
22. Rychak JJ, Graba J, Cheung AM, et al. Microultrasound molecular imaging of vascular endothelial growth factor receptor 2 in a mouse model of tumor angiogenesis. Mol Imaging. 2007; 6:289–96. [PubMed: 18092513]
23. Pagenelli G, Chinol M, Maggiolo M, et al. The three-step pretargeting approach reduces the human anti-mouse antibody response in patients submitted to radioimmunoscintigraphy and radioimmunotherapy. Eur J Nucl Med. 1997; 24:350–351. [PubMed: 9143478]
24. Breitz HB, Weiden PL, Beaumier PL, et al. Clinical optimization of pretargeted radioimmunotherapy with antibody streptavidin conjugate and 90Y-DOTA-biotin. J Nucl Med. 2000; 41:131–140. [PubMed: 10647616]
25. Stieger SM, Dayton PA, Borden MA, et al. Imaging of angiogenesis using Cadence contrast pulse sequencing and targeted contrast agents. Contrast Media Mol Imaging. 2008; 3:9–18. [PubMed: 18335479]
26. Piedra M, Allroggen A, Lindner JR. Molecular imaging with targeted contrast ultrasound. Cerebrovasc Dis. 2009; 27 (Suppl 2):66–74. [PubMed: 19372662]
27. Dayton P, Rychak JJ. Molecular ultrasound imaging using microbubble contrast agents. Frontiers in Bioscience. 2007:19.

28. Zhao S, Kruse DE, Ferrara KW, Dayton PA. Selective imaging of adherent targeted ultrasound contrast agents. Phys Med Biol. 2007; 52:2055–72. [PubMed: 17404455]
29. Hu X, Zheng H, Kruse D, et al. A Sensitive TLRH Targeted Imaging Technique for Ultrasonic Molecular Imaging. IEEE Trans Ultrason Ferroelectr Freq Control. 2010; 57:305–16. [PubMed: 20178897]
30. Couture O, Sprague MR, Cherin E, et al. Reflection from bound microbubbles at high ultrasound frequencies. IEEE Trans Ultrason Ferroelectr Freq Control. 2009; 56:536–45. [PubMed: 19411212]
31. Lyshchik A, Fleischer AC, Huamani J, et al. Molecular imaging of vascular endothelial growth factor receptor 2 expression using targeted contrast-enhanced high-frequency ultrasonography. J Ultrasound Med. 2007; 26:1575–86. [PubMed: 17957052]
32. Bachmann C, Klibanov AL, Olson TS, et al. Targeting mucosal addressin cellular adhesion molecule (MAdCAM)-1 to noninvasively image experimental Crohn's disease. Gastroenterology. 2006; 130:8–16. [PubMed: 16401463]
33. Borowsky AD, Namba R, Young LJ, et al. Syngeneic mouse mammary carcinoma cell lines: two closely related cell lines with divergent metastatic behavior. Clin Exp Metastasis. 2005; 22:47–59. [PubMed: 16132578]
34. Phillips P. Contrast Pulse Sequences (CPS): Imaging non-linear microbubbles. IEEE Ultrason Symp. 2001:1739–45.
35. Zhao S, Kruse DE, Ferrara KW, Dayton PA. Selective imaging of adherent targeted ultrasound contrast agents. Phys Med Biol. 2007; 52:2055–72. [PubMed: 17404455]
36. Willmann JK, Lutz AM, Paulmurugan R, et al. Dual-targeted contrast agent for US assessment of tumor angiogenesis in vivo. Radiology. 2008; 248:936–44. [PubMed: 18710985]
37. Weller GE, Wong MK, Modzelewski RA, et al. Ultrasonic imaging of tumor angiogenesis using contrast microbubbles targeted via the tumor-binding peptide arginine-arginine-leucine. Cancer Res. 2005; 65:533–9. [PubMed: 15695396]
38. Xuan JW, Bygrave M, Valiyeva F, et al. Molecular targeted enhanced ultrasound imaging of flk1 reveals diagnosis and prognosis potential in a genetically engineered mouse prostate cancer model. Mol Imaging. 2009; 8:209–20. [PubMed: 19728975]
39. Lee DJ, Lyshchik A, Huamani J, et al. Relationship Between Retention of a Vascular Endothelial Growth Factor Receptor 2 (VEGFR2)-Targeted Ultrasonographic Contrast Agent and the Level of VEGFR2 Expression in an In Vivo Breast Cancer Model. J Ultrasound Med. 2008; 27:855–866. [PubMed: 18499845]
40. Jun HY, Park SH, Kim HS, et al. Long residence time of ultrasound microbubbles targeted to integrin in murine tumor model. Acad Radiol. 2010; 17:54–60. [PubMed: 19815430]
41. Dayton PA, Pearson D, Clark J, et al. Ultrasonic analysis of peptide- and antibody-targeted microbubble contrast agents for molecular imaging of alphavbeta3-expressing cells. Mol Imaging. 2004; 3:125–34. [PubMed: 15296677]
42. Stieger SM, Dayton PA, Borden MA, et al. Imaging of angiogenesis using Cadence contrast pulse sequencing and targeted contrast agents. Contrast Media Mol Imaging. 2008; 3:9–18. [PubMed: 18335479]
43. Alon R, Bayer EA, Wilchek M. Cell-adhesive properties of streptavidin are mediated by the exposure of an RGD-like RYD site. Eur J Cell Biol. 1992; 58:271–279. [PubMed: 1425765]
44. Klibanov AL, Rasche PT, Hughes MS, et al. Detection of individual microbubbles of an ultrasound contrast agent: fundamental and pulse inversion imaging. Acad Radiol. 2002; 9 (Suppl 2):S279–81. [PubMed: 12188248]
45. Sboros V. Response of contrast agents to ultrasound. Adv Drug Deliv Rev. 2008; 60:1117–36. [PubMed: 18486270]
46. Kaufmann BA, Carr CL, Belcik T, et al. Effect of Acoustic Power on In Vivo Molecular Imaging With Targeted Microbubbles: Implications for Low-Mechanical Index Real-Time Imaging. J Am Soc Echocardiogr. 2009
47. Miller DL, Dou C. Membrane damage thresholds for pulsed or continuous ultrasound in phagocytic cells loaded with contrast agent gas bodies. Ultrasound Med Biol. 2004; 30:405–11. [PubMed: 15063523]

48. Miller DL, Quddus J. Diagnostic ultrasound-induced membrane damage in phagocytic cells loaded with contrast agent and its relation to Doppler-mode images. IEEE Trans Ultrason Ferroelectr Freq Control. 2002; 49:1094–102. [PubMed: 12201456]

49. Samuel S, Fowlkes JB, Miller DL. An in vitro study of the correlation between bubble distribution, acoustic emission, and cell damage by contrast ultrasound. IEEE Trans Ultrason Ferroelectr Freq Control. 2009; 56:589–99. [PubMed: 19411217]

50. van Der Wouw PA, Brauns AC, Bailey SE, et al. Premature ventricular contractions during triggered imaging with ultrasound contrast. J Am Soc Echocardiogr. 2000; 13:288–94. [PubMed: 10756246]

51. Vancraeynest D, Kefer J, Hanet C, et al. Release of cardiac bio-markers during high mechanical index contrast-enhanced echocardiography in humans. Eur Heart J. 2007; 28:1236–41. [PubMed: 17409107]

52. Wolfrum B, Mettin R, Kurz T, Lauterborn W. Observations of pressure-wave-excited contrast agent bubbles in the vicinity of cells. Applied Physics Letters. 2002; 81:5060–62.

53. Wu Y, Zhang X, Xiong Z, et al. microPET imaging of glioma integrin {alpha}v{beta}3 expression using (64)Cu-labeled tetrameric RGD peptide. J Nucl Med. 2005; 46:1707–18. [PubMed: 16204722]

54. Anderson CR, Rychak JJ, Backer M, et al. scVEGF Microbubble Ultrasound Contrast Agents: A Novel Probe for Ultrasound Molecular Imaging of Tumor Angiogenesis. Invest Radiol. 2010; 45:412.

55. Kim DH, Klibanov AL, Needham D. The Influence of Tiered Layers of Surface-Grafted Poly(ethylene glycol) on Receptor Ligand-Mediated Adhesion between Phospholipid Monolayer-Stabilized Microbubbles and Coated Glass Beads. Langmuir. 2000; 16:2808–2817.

56. Sancey L, Garanger E, Foillard S, et al. Clustering and internalization of integrin alphavbeta3 with a tetrameric RGD-synthetic peptide. Mol Ther. 2009 May; 17(5):837–43. [PubMed: 19259068]

57. Takalkar AM, Klibanov AL, Rychak JJ, et al. Binding and detachment dynamics of microbubbles targeted to P-selectin under controlled shear flow. J Control Release. 2004; 96:473–482. [PubMed: 15120903]

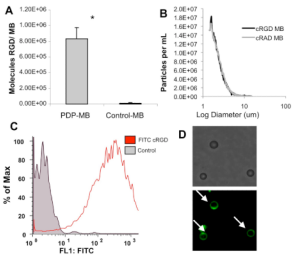

Figure 1.

Characterization of cRGD-bearing microbubbles. (A) Density of fluorescently labeled cRGD peptide on the surface of the microbubble was measured with fluorescence spectroscopy. (B) Size distribution (by number) of cRGD and cRAD control microbubbles, measured by electrozone sensing. (C) Fluorescence histogram generated by flow cytometry of unlabelled control and FITC-cRGD bearing microbubbles demonstrates significant peptide bound to microbubbles. (D) Fluorescently-labeled cRGD on the microbubble surface is shown by epifluorescence microscopy. Microbubbles are denoted by white arrows. Data are presented as mean +/− standard deviation for n=4 independent experiments. *$p<0.01$.

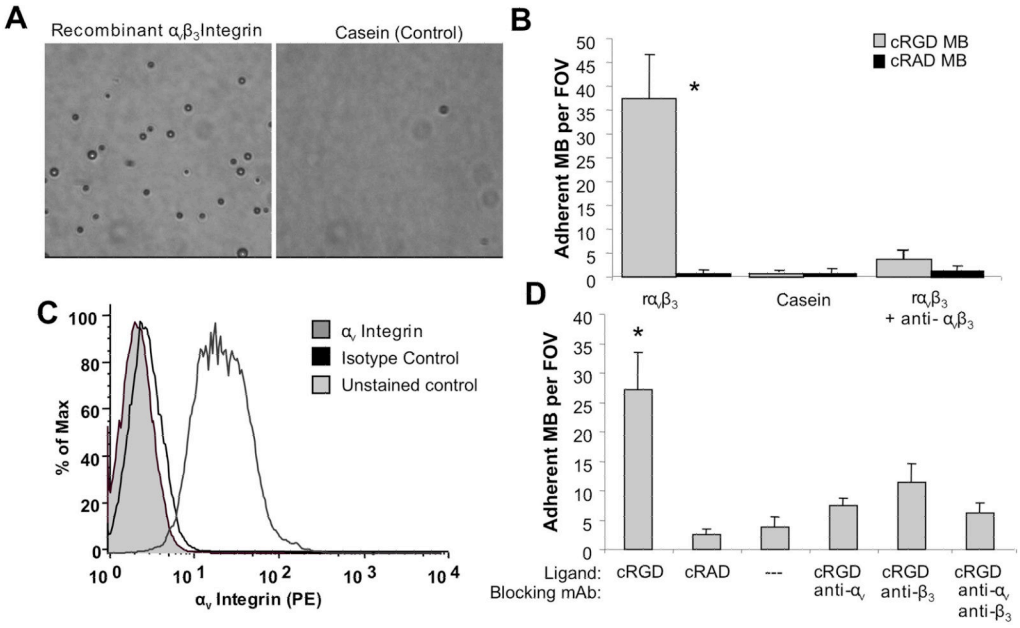

Figure 2.

In vitro microbubble adhesion assays. (A) Characteristic microscopic fields of view for cRGD-MB on recombinant $\alpha_v\beta_3$ integrin (left) and casein (right) surfaces. (B) Functional adhesion of cRGD and control cRAD microbubbles to recombinant $\alpha_v\beta_3$ integrin at a wall shear stress of 1.0 dyne/cm^2. Adhesion of cRGD-MB was significantly reduced in the presence of an anti- $\alpha_v\beta_3$ integrin antibody. (C) Flow cytometry results demonstrating $\alpha_v\beta_3$ integrin expression on bEND.3 murine endothelial cells. (D) Functional adhesion of cRGD and control cRAD microbubbles to bend.3 cells at 1.0 dyn/cm^2 in the presence of blocking antibodies against various subunits of $\alpha_v\beta_3$ integrin. Data are presented as mean +/− standard deviation for n=5 independent experiments. *$p<0.01$ versus all negative control conditions.

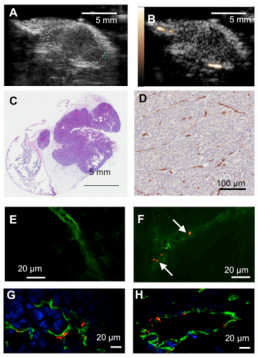

Figure 3.

Characterization of Met-1 model of mammary carcinoma in mouse. Representative ultrasound images of tumors two weeks after inoculation in (A) B-mode and (B) CPS mix mode without microbubbles. (C) H&E staining shows morphology of tumor and adjacent tissue. (D) Representative field of view showing CD31 expression by immunohistochemistry in tumor. (E)-(F) Representative confocal fluorescence images of tumor sections after administration of FITC-lectin in the absence (E) and presence (F) of DiI-labeled cRGD microbubbles. Green color (FITC-lectin) delineates endothelium, and fluorescently-labeled MB (DiI) are shown in red (arrows). (G) – (H) Confocol fluorescence images of immunohistochemical sections showing CD31 (green), $\alpha_v\beta_3$ integrin (red), and DAPI (blue).

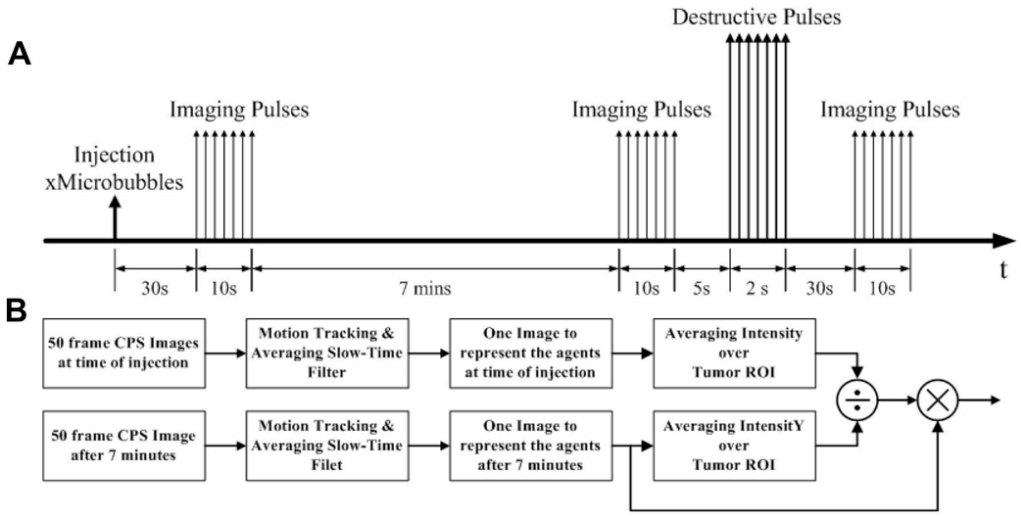

Figure 4.

Schematic showing contrast ultrasound imaging strategy and quantitative image analysis. (A) ten-second sequences of images were acquired in CPS mode immediately after MB administration, after a seven-minute dwell period, and after MB destruction. (B) Image sequences were processed offline to determine the average image intensity within regions of interest.

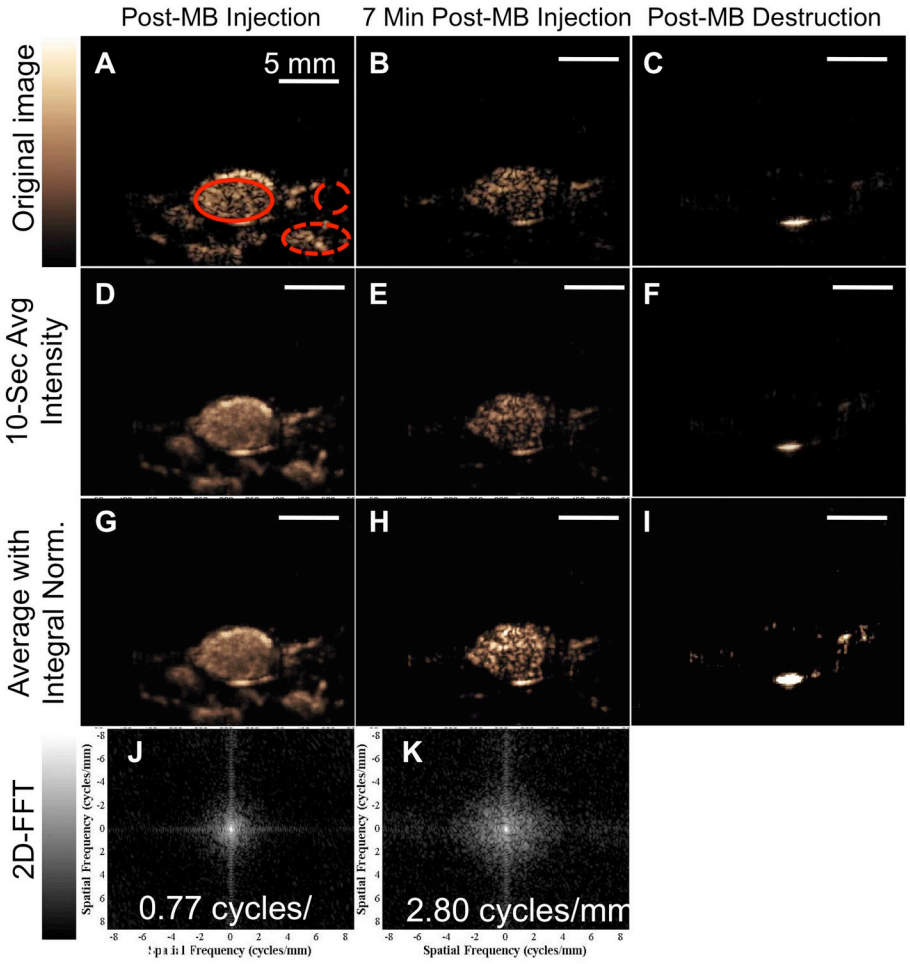

Figure 5.

Analysis of contrast ultrasound imaging with cRGD-MB. (A-C) Representative single frame contrast US images (A) immediately after cRGD-MB administration. (B) after a seven-minute dwell period, and (C) after cRGD-MB destruction. Regions of interest are indicated as follows: Solid circle indicates tumor; wide dashed circle indicates adjacent tissue; and narrow dashed circle indicates the feeding blood vessel (D-F) Images corresponding to time points in A-C were averaged over 50 frames in over to suppress the echoes from circulating MB. (G-I) Images from D-F were normalized to match the spatially-integrated intensity from the time of injection with the spatial integral after the seven-minute circulation, demonstrating differences in speckle between the time of injection and after accumulation. (J-K) 2D-Fourier transform further differentiates adherent MB from circulating MB. (J) Image Fourier transform from time of injection has 0.77 cycle/mm −6 dB width. (K) Image Fourier transform after seven minutes has 2.8 cycle/mm −6 dB width due to speckle.

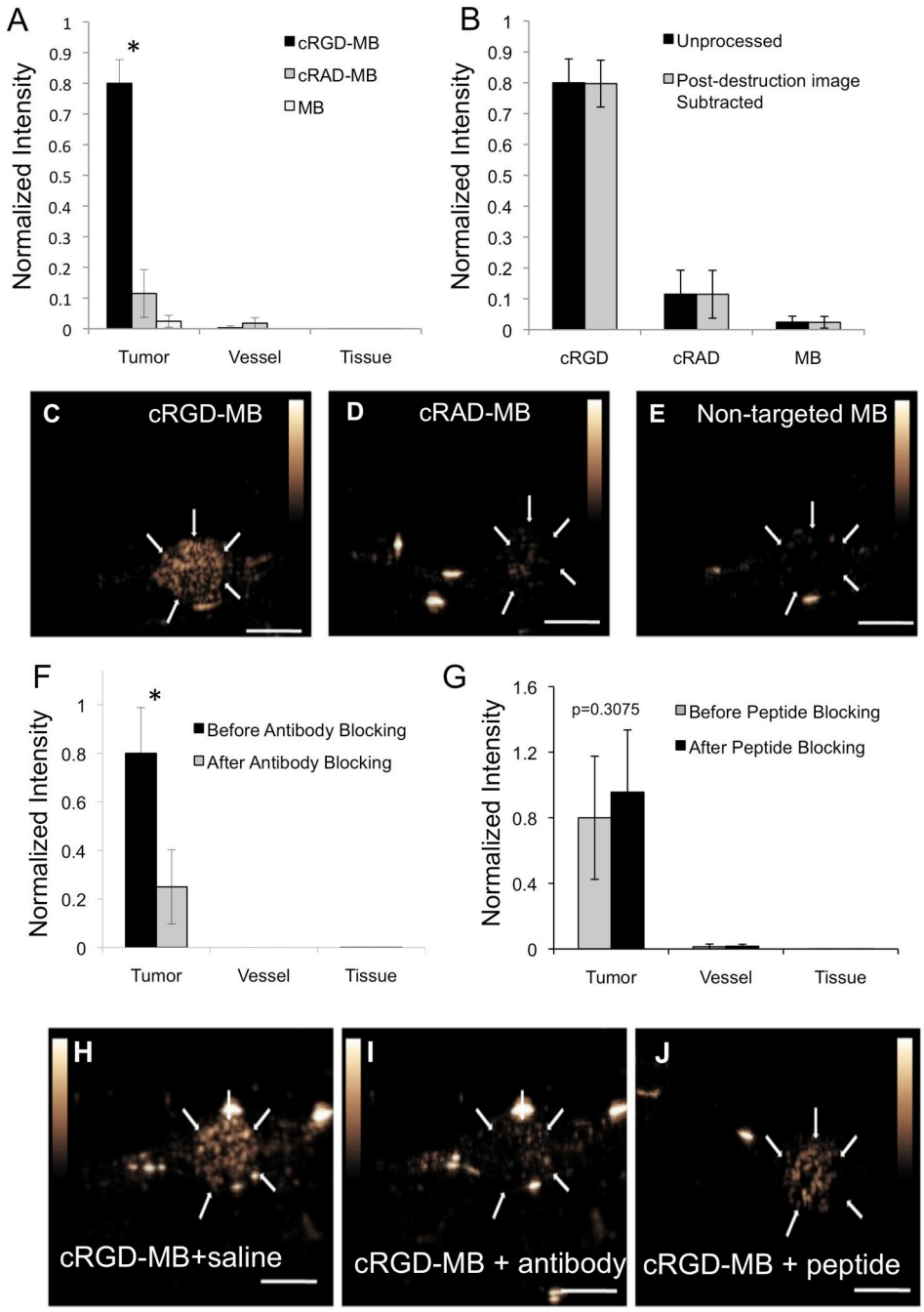

Figure 6.

Specificity of cRGD-MB adhesion *in vivo* (A) Normalized image intensities of cRGD, cRAD and non-targeted MB at 7 minutes within tumor, vessel and adjacent tissue regions, respectively. *$p<0.03$ for cRGD-MB in tumor relative to all other conditions. (B) Normalized intensities of cRGD, cRAD and non-targeted MB are compared before and after subtraction of the post-destruction image. Representative images of (C) cRGD, (D) cRAD and (E) non-targeted microbubbles at the 7-minute time point. Normalized intensities before and after administration of a blocking antibody (F) or soluble peptide (G). Representative images for pre-administration of saline (H), pre-administration of blocking antibody (I), and

pre-administration of soluble peptide (J) at 7-minute time point. Scale bars represent 5 mm * $p<0.01$

Table 1

Summary parameters of targeted and control microbubbles measured by electrozone sensing. All measurements represent mean +/− standard deviation of 3 repeats of samples from the same batch.

	cRGD-MB	cRAD-MB
Mean Diameter (um)	2.75 +/− 0.02	2.71 +/− 0.01
Median Diameter (um)	2.82 +/− 0.00	2.79 +/− 0.03
Concentration ($\times 10^7$ mL^{-1})	148 +/− 1.1	133 +/− 8.0
Area Concentration ($\times 10^8$ um^2/mL)	146 +/− 6.6	121 +/− 7.2